Title: Synaptic and intrinsic mechanisms underlying development of cortical direction selectivity

Abbreviated title: Mechanisms of direction selectivity

Authors: Arani Roy[1,2], Jason J. Osik[1,2], Benyamin Meschede-Krasa, Wesley Alford, Daniel P. Leman, Stephen D. Van Hooser[1,2,3*]

1: Department of Biology
2: Volen Center for Complex Systems
3: Sloan-Swartz Center for Theoretical Neurobiology
Brandeis University, Waltham, MA 02454 USA

Corresponding author:
*Stephen D. Van Hooser, vanhoosr@brandeis.edu
Brandeis University, 415 South St. MS008, Waltham, MA 02454 USA

Number of Pages: 48
Number of Figures and Tables: 7 Figures, 1 Table

Conflicts of interest: The authors declare no competing financial interests.

Contributions: AR, JJO, and SDV designed experiments; AR, JJO, BMK, and WA collected data; AR, JJO, DPL, and SDV performed data analysis; AR, JJO, and SDV wrote the manuscript with input from all authors.

Acknowledgements: We thank Zoey Keeley and Daniel Shin for help with figure layout, and members of the Van Hooser lab for comments and feedback during the project and on the manuscript.

Keywords: primary visual cortex; direction selectivity; cortical development; sensory experience; spatiotemporal receptive fields; intrinsic excitability; spike threshold.

Abstract

Some neural circuits are constructed through an overproduction of initial connections followed by activity-dependent refinement. Under this paradigm, functional receptive fields would be expected to be narrowed from a diffuse immature condition to a sharper mature condition. Alternatively, neural activity might lead to formation of new connections, leading to expansion of an initially compact receptive field. In the simple cells of the ferret visual cortex undergoing developmental enhancement of direction selectivity, we found evidence for a mixed mechanism: an expansion of the spatiotemporal receptive fields along the temporal dimension combined with a narrowing in space-time through a marked loss of inputs with certain space-time selectivities. Further, the resulting increase in subthreshold direction selectivity was accompanied by increases in near-spike-threshold excitability and input-output gain that resulted in dramatically increased spiking responses. Increases in subthreshold membrane responses and the increased input-output spiking gain were both necessary to explain firing rates in experienced ferrets. These results demonstrate that cortical direction selectivity develops through a combination of plasticity in synaptic and cell-intrinsic properties.

Introduction

A major principle of developmental neuroscience is the concept of initial overproduction of connections followed by activity-dependent pruning (Brown et al., 1976; Changeux and Danchin, 1976; Huttenlocher, 1979; Purves and Lichtman, 1980; Miller et al., 1989; Petanjek et al., 2011). At the neuromuscular junction, for example, muscle fibers are initially innervated by multiple motor neuron axons, and these connections are paired back through competitive, activity-dependent processes so that each muscle fiber is ultimately innervated by just a single motor neuron axon (Brown et al., 1976). Functionally, overproduction of inputs should produce receptive or motor fields that are initially broad and diffuse and that become selective as synapses are pruned by correlational processes that depend on the animal's own experiences (Miller et al., 1989).

It is unclear if synaptic overproduction followed by pruning underlie the development of response selectivities in the mammalian visual cortex (V1). At the time of eye opening, neurons in ferret and primate V1 respond selectively to edges oriented at specific angles (orientation selectivity), but respond about equally to motion in the two opposite directions orthogonal to the preferred axis of orientation. Selectivity to direction of motion (direction selectivity) develops rapidly in the days and weeks after the onset of visual experience (Hatta et al., 1998; Li et al., 2006; Clemens et al., 2012; Smith et al., 2015), and can be accelerated in the lab through experience with moving stimuli (Li et al., 2008; Van Hooser et al., 2012). In cats and primates, it has been demonstrated that a set of inputs activating the cell at varying spatial positions and temporal latencies following a specific spatiotemporal order underlies direction selectivity in the visually mature state (DeAngelis et al., 1993a; Jagadeesh et al., 1993; McLean et al., 1994; Livingstone, 1998). But it remains unclear how this very precise spatiotemporal pattern emerges

during development. One might hypothesize, in analogy with the diffuse connectivity in the neuromuscular junction, that the early unselective state (for direction) could reflect the presence of broad, diffuse initial pattern of spatiotemporal inputs that are later pruned by activity-dependent processes to eliminate responses to inappropriate directions and speeds. Alternatively, spatiotemporal receptive fields may be initially compact and then obtain selectivity, at least in part, by expanding with experience.

To distinguish between these two ideas, we carried out in vivo intracellular recordings in V1 from two groups of ferrets at different stages of visual development: visually naïve (post-natal day P30-34) and visually experienced (P40-60). Using reverse correlation of membrane potential (Vm) responses to sparse white noise stimuli, we constructed the spatiotemporal receptive fields (STRF) of neurons in the two groups and compared them. We found that receptive fields in the naïve state exhibited spatiotemporally compact ON and OFF subfields, which in the experienced animals became more elongated along the temporal axis, corroborating the idea of recruitment of new synaptic inputs. However, the subunits also became significantly narrower along their preferred space-time axis, consistent with pruning of synaptic inputs with certain spatiotemporal properties. Thus, our results provide evidence for a mixed mechanism in which synaptic pruning is accompanied by formation of some new synaptic inputs, ultimately resulting in receptive field structures that exhibit markedly increased direction selectivity.

Surprisingly, the enhancement in Vm responses brought about by these rearrangements of spatiotemporal inputs did not successfully predict the developmental enhancement in spiking responses. We argued that a concomitant developmental alteration in intrinsic excitability, which gates the input-output transformation of neurons, could underlie this discrepancy. Consistent with this idea, we found that V1 neurons in visually experienced animals had stronger gains in

Vm-to-spike transformation, and that this gain enhancement was accompanied by a lowering of spike threshold. Changes in subthreshold responses and voltage-to-firing rate gain enhancement both had to be considered to explain the total increases in firing rates that are observed over this period (Clemens et al., 2012), signifying that a combination of synaptic and intrinsic plasticity mechanisms underlie development of direction selectivity.

Results

At the time of eye opening, around 30-33 days of postnatal age (P30-P33), neurons in ferret visual cortex exhibit robust selectivity for stimulus orientation but only very weak selectivity for stimulus direction (Li et al., 2006; Li et al., 2008). Selectivity for stimulus direction emerges over the weeks following eye opening through a process that requires visual experience (Li et al., 2006). In cortical simple cells in the visually experienced state, direction selectivity is thought to arise from spatiotemporally selective inputs activating the cell at varying spatial positions and temporal latencies (DeAngelis et al., 1993a; Jagadeesh et al., 1993; McLean et al., 1994; Livingstone, 1998). According to this model (Reichardt and Poggio, 1976; Reichardt, 1987), a direction-selective neuron is maximally activated when its inputs selective for specific spatial locations within the receptive field are activated by a moving stimulus in a specific temporal order – with the inputs with the longest latencies activated first and inputs with progressively shorter latencies sequentially activated thereafter. This spatiotemporally sequenced order of activation ensures that the subthreshold inputs activated by the preferred direction of motion arrive at the soma simultaneously and achieve maximal summation, leading to a strong response. In contrast, a stimulus moving in the null direction activates the shortest latencies first followed by progressively longer latencies, thereby leading to suboptimal summation of activity, and consequently lower responses in the postsynaptic neuron. A direction-selective simple cell with its inputs organized in this manner exhibits a stereotypical "slant" in its spatiotemporal receptive field.

One could imagine at least 2 divergent hypotheses for a transition from a responsive but unselective state to a responsive and selective state. The "overproduction and prune" hypothesis would suggest that inputs to the initial receptive field would be broad and diffuse and that

activity-dependent mechanisms would strengthen inputs that were repeatedly activated (Brown et al., 1976; Changeux and Danchin, 1976; Huttenlocher, 1979; Purves and Lichtman, 1980; Miller et al., 1989; Meliza and Dan, 2006; Petanjek et al., 2011; Van Hooser et al., 2014; Ritter et al., 2017). This hypothesis is illustrated with inputs to visual cortical neurons as "Possible Juvenile State I" in **Figure 1**. Another possibility ("Juvenile State II in **Figure 1**) is that these receptive fields start out in a compact spatiotemporal extent, and grow with experience in a manner that is constrained according to experience-independent processes. In this second state, the initial lack of selectivity derives from the space-time symmetry of the compact initial receptive field.

In order to examine the initial state of spatiotemporal receptive fields and to understand how these fields are altered during the short critical period for the emergence of direction selectivity, we carried out *in vivo* intracellular recordings in the visual cortex of anesthetized ferrets using sharp microelectrodes. Intracellular recordings were used because naïve visual cortical neurons exhibit lower firing rates than experienced animals (Clemens et al., 2012; Popovic et al., 2018), and we wanted to be able to examine the receptive field properties of the subthreshold voltage in addition to spiking. Experimental animals were split in to 2 age groups: visually naïve ("naïve": age P30-34, n = 10 animals, 23 cells) and visually experienced ("experienced": age P40-60, n = 11 animals, 29 cells). Drifting sinusoidal grating stimuli were used to measure responses to stimulus orientation and direction. Cells were classified as simple or complex by comparing the fundamental (F1) and the DC components (F0) of the visual responses (Carandini and Ferster, 2000; Mechler and Ringach, 2002; Priebe et al., 2004). We first converted the Vm and spike responses of each recorded neuron to the frequency domain using Fast Fourier Transform (FFT) and then analyzed all response properties for the F0 and F1 components separately as well as combined (F0+F1). We calculated Vm and spike modulation

ratios by dividing the amplitude of the F1 component by that of the F0 component of the respective responses. Cells with spike modulation ratio equal to or greater than 1 were classified as simple, while the rest were categorized as complex (**Supplementary Figure 2-1**). Neurons that did not fire sufficient spikes were classified as simple if their Vm modulation ratio was greater than 0.5. According to this classification, our dataset contained 10 simple and 13 complex cells in the naïve group, and 16 simple and 13 complex cells in the experienced group. After a cell's orientation and direction preferences were identified by the responses to grating stimuli, sparse noise bar stimuli were shown to examine the spatiotemporal receptive fields only for the simple cells, because such analysis of linear summation properties apply only to simple cells.

Emergence of enhanced direction selectivity following visual experience

We constructed orientation and direction tuning curves from recorded Vm and spiking activities in response to sinusoidal gratings. **Figure 2AB** shows an example simple cell each from a naïve and an experienced ferret. The neuron from the naïve ferret (**Figure 2AB**, left panel) responded strongly to horizontal gratings, irrespective of whether they were moving upward or downward, while showing only weak subthreshold responses to vertical gratings. In contrast, the neuron from the experienced ferret (**Figure 2AB**, right panel) strongly responded only to vertical gratings drifting to the right while responding minimally to all other stimuli. Direction selectivity index values for spiking activity and Vm were much larger for the experienced example cell than for the naïve cell. On average, the experienced cells exhibited stronger direction selectivity compared to the naïve cells, both at the subthreshold Vm and the suprathreshold spiking levels (**Figure 2C**, Direction selectivity index or DSI. Top, Vm: naïve: mean = 0.16 ± 0.02, n = 23;

experienced: mean = 0.35 ± 0.04, n = 29; p <0.001, WRS test; bottom, spike: naïve: mean = 0.3 ± 0.05, n = 14 (9 cells did not spike); experienced: mean = 0.66 ± 0.05, n = 29; p <0.001, WRS test).

In a majority of cells, the DSI for spiking responses were greater than the DSI for Vm responses. A pairwise comparison of Vm and spike DSI within each neuron revealed that the spike DSI was significantly higher than Vm DSI in both the naïve and the experienced groups (**Figure 2D**; naïve, p = 0.001, n = 14; experienced, p < 0.001, n = 29; signed rank test). Thus, in both groups, the outputs of V1 cells were more sharply tuned for direction than their summed inputs. Also, to test if the developmental enhancement of DSI in V1 cells were restricted to the mean (F0) or the modulated (F1) component or affected both, we calculated DSI separately for the F0 and the F1 response components. F0 and F1 DSI for both sub- and suprathreshold responses in the experienced group were significantly higher than the naïve group (**Figure 2E**; F0: Vm: naïve: mean = 0.15 +/- 0.02, n = 23; experienced: mean = 0.27 +/- 0.04, n = 29; p = 0.02, WRS test; spike: naïve: mean = 0.33 +/- 0.05, n = 14; experienced: mean = 0.62 +/- 0.05, n = 29; p = 0.003, WRS test; F1: Vm: naïve: mean = 0.32 +/- 0.04, n = 14; experienced: mean = 0.57 +/- 0.04, n = 29; p < 0.001, WRS test; spike: naïve: mean = 0.31 +/- 0.06, n = 14; experienced: mean = 0.7 +/- 0.04, n = 29; p < 0.001, WRS test), demonstrating that both the mean and the modulated component of visual responses became more direction-selective during development.

An increase in direction selectivity index values could be realized either by an increase in responses to the preferred direction, a decrease in responses to the null direction, or both. To distinguish between these possibilities, we analyzed the Vm and spiking response amplitudes to the preferred and the null direction stimuli for each cell. The total (F0 plus F1) responses to the

preferred and null stimuli were compared between the naïve and experienced groups, separately for Vm and spiking responses (**Figure 2F**). At the level of Vm (**Figure 2F**, top), the null responses (left) did not show any significant change over development, whereas the preferred responses (right) showed a modest but significant increase from the naïve to the experienced group (Null, naïve: mean = 11 ± 1.2, n = 23; experienced: mean = 11.2 ± 0.9, n = 29, p = 0.8, WRS test; Preferred, naïve: mean = 13.1 ± 1.3, n = 23; experienced: mean = 17.3 ± 0.9, n = 29, p = 0.008, WRS test). At the level of spiking (**Figure 2F**, bottom), both the null and the preferred responses underwent developmental enhancement (null, naïve: mean = 4.8 ± 1.2, n = 23; experienced: mean = 9 ± 1.5, n = 29, p = 0.01, WRS test; preferred, naïve: mean = 6.6 ± 1.6, n = 23; experienced: mean = 24.7 ± 2.6, n = 29, p < 0.001, WRS test). Therefore, the increase in direction selectivity following visual experience was driven primarily by a robust increase in responses to the preferred direction of motion and not by a decrease in response to the null direction of motion. Notably, while this increase in response to the preferred direction was modest (32%) at the Vm level, it was dramatic for spiking activity (274%).

Reorganization of simple cell spatiotemporal receptive fields following visual experience

The increase in Vm responses to the preferred direction raises the question as to what changes in the spatiotemporal receptive field configurations might underlie these increases. To compare spatiotemporal receptive field structures of the Vm responses between simple cells from the naïve and experienced groups, we performed reverse correlation of the response of the Vm to sparse, 1-dimensional white noise visual stimulation (Reid et al., 1987, 1991; Reid et al., 1997; Ringach et al., 1997; Priebe and Ferster, 2005; Rust et al., 2005; van Kleef et al., 2010). The noise stimulus consisted of black, white and gray bars, angled at the cell's preferred orientation,

that changed pattern every 100 milliseconds (**Figure 3A**). Positive cross-correlation values were obtained if a white bar (contrast 1) led to increased Vm or a black bar (contrast -1) led to decreased Vm (ON subunit), and negative cross-correlation values were obtained if a white bar led to decreased Vm or a black bar led to increased Vm (OFF subunit). For every spatial location, the cross-correlation values were plotted at varying lag times, thereby allowing assessment of the latencies at which the high or low cross-correlation values were obtained. Because visually driven spiking activity was weak in naïve ferrets, we focused our analysis primarily on the Vm responses, for which a reliable spatiotemporal receptive field could be computed for every simple cell tested.

Figure 3BC shows Vm spatiotemporal receptive fields of 4 cells recorded from a naïve ferret and 4 cells recorded from an experienced ferret. Consistent with previous findings (Reid et al., 1987, 1991; DeAngelis et al., 1993a; Priebe and Ferster, 2005), the spatiotemporal receptive field subunits from direction-selective neurons in experienced animals were slanted in space-time. For cell #60, gratings moving from right to left on the monitor would activate the inputs with longer latencies first, progressively moving to shorter latencies as the grating moves across the visual field, thereby leading to maximal response. Stimuli moving from left to right, on the other hand, will activate the shorter latency inputs followed by the longer latency inputs, thereby leading to sub-optimal responses. The spatiotemporal receptive field of Cell #86 was also slanted, albeit in the opposite direction.

The spatiotemporal receptive fields from the neurons in naïve animals were not completely unstructured, and exhibited several properties of neurons from experienced animals such as alternating ON and OFF subunits and a small slant in space-time. However, the subunits

from the experienced cells were longer and narrower in profile, and relatively more slanted in space-time.

To rigorously quantify the degree to which subunit structure differed between naïve and experienced animals, we fitted ellipses to the individual ON and OFF subunits (Leong et al., 2016) and compared several shape parameters of these ellipses (see **Materials and Methods**). We chose a set of 9 parameters that adequately captured the relevant spatial and temporal characteristics of the receptive fields (**Figure 4A**) – 'eccentricity': eccentricity of the fitted ellipse; 'major axis': the length of the major axis of the fitted ellipse; 'minor axis': the length of the minor axis of the fitted ellipse; 'orientation': the angle the ellipse subtended on the space (x-) axis; 'area': the full area covered by the ellipse, in pixels; 'spatial extent': projection of the ellipse on the space axis; 'temporal extent': projection of the ellipse on the time/latency axis; 'minimum latency': the lower bound of the fitted ellipse on the time axis signifying the shortest latency response; and 'maximum latency': the upper bound of the fitted ellipse on the time axis signifying the longest latency response. Wilcoxon rank sum test comparisons revealed that 6 out of these 9 parameters were significantly different between the naïve and the experienced groups: eccentricity, major axis, minor axis, orientation, temporal extent and minimum latency. The shape parameter that is most relevant to direction selectivity is the eccentricity of the ellipses describing the subunits. If subunits are broad along the minor axis of the ellipse, they will enable some response summation from stimuli moving in either direction, thus leading to weaker direction selectivity. Also, if subunits are short along the major axis of the ellipse, there might not exist sufficient latency differences to facilitate differential input summation. Therefore, to optimally support high direction selectivity, receptive field subunits would have to be narrow on the minor axis and elongated on the major axis, which would result in high eccentricity.

Consistent with this idea, we found that the eccentricity measured from the experienced subunits were significantly higher ($p < 0.001$), and was caused by both a longer major axis ($p < 0.03$) and a shorter minor axis ($p < 0.03$, **Figure 4A**). Also, the subunits from the experienced animals subtended a smaller angle on the space axis (orientation: $p < 0.005$), which would indicate that the cells from experienced animals are tuned to higher motion velocities, consistent with data from actual V1 recordings in cats (DeAngelis et al., 1993b). The overall area ($p < 0.6$) and the spatial projection ($p < 0.35$) of the subunits did not significantly differ. However, the projection on the latency axis was significantly longer in the experienced group ($p < 0.04$), suggesting that a longer range of response latencies became available in the experienced animals. This extension of the latency range was achieved solely by stretching the receptive field subunits towards the lower latency side: while the maximum latencies of the subunits were not significantly different ($p < 0.3$), the minimum latencies were significantly lower in the experienced group ($p < 0.05$). This suggests recruitment of shorter-latency inputs in the experienced animals. Consistent with this view, we found that the Vm response latency distributions were significantly shifted towards shorter latencies in the experienced animals (**Figure 4E**), and these results mirror reduced latencies observed in experienced vs. naïve neurons in ferret lateral geniculate nucleus (Tavazoie and Reid, 2000).

If the changes in Vm spatiotemporal receptive field structure resulted in improved discrimination between the preferred and null directions of motion, then the receptive field structure parameters should correlate with Vm direction index measured in each cell. Therefore, we computed linear correlations between cell-averaged shape parameters and the cells' Vm direction index values (**Figure 4B**). We found that the Vm direction index of the cells increased with increasing 'narrowness' of the subunits (longer 'major axis', shorter 'minor axis' and higher

‘eccentricity’) and decreasing minimum latencies accessible (lower ‘min latency’). Other parameters did not show significant correlation. These data further corroborate the idea that narrower spatiotemporal input profiles and availability of shorter-latency inputs exert a strong impact on directional summation of inputs in simple cells of experienced animals, thereby leading to higher direction selectivity. The subunit shapes for all cells are shown in **Figure 4CD**.

In sum, following visual experience, the Vm receptive fields exhibited marked reorganization involving increased eccentricity of the space-time profile and recruitment of lower latency inputs, leading to improved discrimination of directional inputs at subthreshold level and thus a more direction-selective Vm response.

Plasticity of cellular intrinsic properties following visual experience

We saw a sharp rise in visually-evoked spiking responses in the experienced animals. The fraction of cells that fired action potentials in response to drifting grating stimuli was significantly higher in the experienced group (simple: naïve, 7/10; experienced, 16/16; $p < 0.05$, complex: naïve, 7/13; experienced, 13/13; $p < 0.05$, Fisher Exact test). Thus, every recorded cell in the experienced group fired action potentials, but 9/23 cells in the naïve group did not fire any action potentials at all. However, enhancement of Vm responses mediated by reorganization of STRF structure alone could not account for this enhanced spiking. As we saw in **Figure 2F**, the responses to the preferred direction underwent modest developmental increase (32%) at the Vm level, but the increase was dramatic for spiking activity (274%). Therefore, we argued that changes in cell-intrinsic properties also must have played a role in amplifying the effects at the Vm level. Visual inspection of spike waveforms revealed a couple of striking differences between the naïve and the experienced groups: in the naïve group, the spikes were significantly

broader and the take-off point of the action potential (spike threshold) was higher (**Figure 5ABC**). These observations lead us to examine cell-intrinsic properties more carefully.

To characterize changes in cell-intrinsic properties, we examined several parameters of the action potential. These parameters included the maximum rate of change in Vm preceding a spike (max dV/dt), which has been shown to correlate with the density of sodium channels (Colbert and Pan, 2002; Kole et al., 2008; Hu et al., 2009; Grubb and Burrone, 2010; Kuba et al., 2010); a quantity called the spike kink (one way to define threshold), which is based on the time when the voltage obtains a sufficiently large rate-of-change relative to its maximum (Azouz and Gray, 1999); and the full width at half maximum.

In vivo, the maximum dV/dt exhibited a strong increase between naïve and experienced animals (**Figure 5C**, naïve mean: 172.2 ± 64.6 mV/msec, experienced mean: 253 ± 78.3 mV/msec, WRS test p<2.0e-04), a small empirical drop in spike kink voltage (**Figure 5D**, naïve mean: 21 ± 0.4 mV, experienced mean: 19.1 ± 4.7 mV, WRS test p=0.21, not statistically significant), and a very substantial decrease in action potential width (**Figure 5E**, naïve mean: 1.6 ± 0.7 msec, experienced mean: 1.0 ± 0.4 msec, WRS test p<4.3e-04).

These *in vivo* measurements of action potential properties are altered by the ongoing activity of the cortex, so we also made these measurements in synaptic transmission-blocked visual cortical slices prepared from naïve and experienced ferrets. Maximum dV/dt measurements in slice (**Figure 5F**) strongly resembled those measured *in vivo* (naïve mean: 162.1 ± 51.1 mV/msec, experienced mean: 264.4 ± 61.9 mV/msec, WRS n vs. e, P<2.4e-05). The spike kink voltage exhibited a small, significant decrease with experience (naïve mean: -25 ± 3.5 mV, experienced mean: -30.2 ± 3.7 mV), consistent with the idea that the experienced cells were more excitable near threshold. As expected for developing animals, input resistance

exhibited a drop with developmental age (naïve mean: 222.9 ± 57.9 MΩ, experienced mean: 144.8 ± 39.3 MΩ), meaning that it took more time to charge older cells from rest than naïve cells, even though the experienced cells exhibited evidence of being more excitable near threshold. As a result of the increased charging time for older cells, firing rate vs. input current curves were not different across the conditions despite the evidence of increased max dV/dt (**Figure 5IJK;** f-I curve Kruskal-Wallis test of linear slopes: $P<0.068$).

Changes in the voltage-to-firing rate transform contribute to development of visual responses

Although we found evidence for changes in excitability with development, the preceding analyses could not tell us quantitatively how these changes might impact sensory responses. To address this, we examined the voltage-to-firing rate transformation following methods of Priebe and Ferster (Priebe et al., 2004; Priebe and Ferster, 2005, 2006). In brief, voltage waveforms were median-filtered to remove spikes (**Figure 6AB**), and both spike trains and spike-trimmed voltage waveforms were binned into 30 msec intervals (**Figure 6C**) to generate pairs of Vm and firing rate observations. Voltage-to-firing rate relationships, with sliding 1mV empirical mean curves and power law fits to the data, are shown for 4 examples cells in **Figure 6DE**. Empirical mean voltage-to-firing rate curves for all naïve and experienced cells are plotted in **Figure 6F**. Generally, most naïve cells exhibited smaller firing rates for a given voltage than the experienced cells, which reflects the increased excitability of the mature neurons. On average, experienced cells exhibited significantly higher firing rates than naïve cells over a wide range of voltages (**Figure 6G**).

To calculate the average impact of changes in selectivity and firing rates due to membrane voltage and the voltage-to-firing rate transform across naïve and experienced cortical

neurons, we modeled the results phenomenologically by passing the actual voltage waveforms that were recorded for each stimulus through each cell's power law fit function to generate firing rate responses on a bin-by-bin basis. This phenomenological model did an excellent job of reproducing the actual firing rates recorded for each stimulus and each cell for both naïve and experienced cells (**Figure 7AB**). To explore the impact of changes in membrane voltage and voltage-to-firing rate transforms separately on the direction index values (**Figure 2**, **Figure 7C**) and firing rates (**Figure 7E**) we observed, we created 10000 bootstrap simulations (Press et al., 1993) of experiments with 20 cells that used the waveforms and voltage-to-firing rate transform for different cell groups. In each simulation, a cell was chosen at random (with replacement) to provide the response Vm waveforms, and another cell was chosen at random (with replacement) to provide the voltage-to-firing rate transform. This rough phenomenological model assumes that voltage responses and gains can be selected independently; in the actual data, these quantities are not completely independent and the random mixture model slightly overestimates actual firing rates from the population. When membrane voltages and voltage-to-firing rate transforms were both selected from naïve cells, the simulations yielded relatively low direction selectivity index values (**Figure 7D**) and low firing rate responses (**Figure 7F**), similar to the actual data (**Figure 2EF** and **Figure 7CE**). Similarly, when these quantities were both selected from experienced cells, the simulations exhibited high direction selectivity and higher firing rates as in the actual data (**Figure 2EF** and **Figure 7CE**). Applying the experienced voltage waveforms to naïve voltage-to-firing rate transforms resulted in a big increase in direction selectivity, even larger than those measured in mature animals (**Figure 7CD**), but the simulated firing rates were below those measured in the actual experienced animals (**Figure 7EF**). Applying the naïve voltage waveforms to experienced voltage-to-firing rate transforms did not produce substantial increases

in direction selectivity compared to the naïve case, although firing rates were elevated. Therefore, changes in the underlying selectivity of the voltage waveforms from naïve to experienced was sufficient to confer increased direction selectivity values across these conditions, but the increased gain of the experienced voltage-to-firing rate transforms were needed to also confer the higher firing rates observed in experienced animals (**Figure 7CDEF**).

Discussion

We studied the evolution of spatiotemporal receptive fields, excitability, and voltage-to-firing rate transformations over a short period of rapid visual development of direction selectivity in ferret visual cortex. Shape analysis of linear spatiotemporal receptive fields of simple cells showed that the elliptical subunits in experienced animals exhibited more eccentric profiles and contained energy at shorter latencies not seen in naïve animals, signifying pruning of some inputs as well as recruitment of other new inputs. This reorganization led to a significant increase in direction selectivity at the level of membrane voltage. Neurons in experienced animals exhibited hallmarks of increased cell-intrinsic excitability, such as a lower spike threshold. When analyzed with system-response methods, we found that these changes in excitability contributed to a substantial increase in the voltage-to-firing rate transform with experience. The full extent of increases in spiking activity could only be explained by considering both the enhancement in Vm responses and the enhancement of input-output gain.

Extension and refinement of spatiotemporal receptive fields

In the developing visual system, molecular cues and spontaneous activity (Katz and Shatz, 1996) shape the formation of initial circuitry and the emergence of initial cortical receptive field properties, including retinotopic organization (Cang et al., 2008) and orientation selectivity (Chapman and Stryker, 1993; Crair et al., 1998; Li et al., 2006; Smith et al., 2018) (although not its alignment across the 2 eyes, which requires experience (Wang et al., 2010; Gu and Cang, 2016; Whitney et al., 2019)). In cortex of ferrets (Li et al., 2006) and primates (Hatta et al., 1998) (but not mice: (Rochefort et al., 2011)), selectivity for direction of motion is not

present at eye opening – neurons respond about equally to stimulation in 2 opposite directions – but develops over a period of about 2 weeks in ferrets and about 4 weeks in macaques.

The question of how a neural system can be responsive to a wide stimulus set and then become more restricted with experience reminds one of the "overproduction and pruning" hypothesis (Brown et al., 1976; Huttenlocher, 1979; Purves and Lichtman, 1980; Petanjek et al., 2011), also called the "stabilization" hypothesis (Changeux and Danchin, 1976). One might imagine that the connections that support multiple responses are present initially, and then, with activity-dependent development, "inappropriate" connections are pruned away and reinforced connections are strengthened. Alternatively, an early compact receptive field could become extended with visual experience, through addition of new inputs. Here, we found evidence for a reorganization process that combines some elements of both mechanisms. On the one hand, the mature receptive fields became elongated along the temporal axis, particularly by recruiting new inputs with shorter response latencies that did not exist in the naïve state. These results fit nicely with prior anatomical observations that the number of synapses being formed in ferret and human visual cortex during this time are greatly increasing (Huttenlocher, 1990; Durack and Katz, 1996; Ruthazer and Stryker, 1996; White et al., 2001; Erisir and Harris, 2003; White and Fitzpatrick, 2007), and suggest that precise growth may be an important principle of the development of some neural circuits. However, the mature receptive fields also became significantly narrow in space-time, which signify that inputs with certain spatiotemporal properties were discarded during development, providing evidence for the pruning mechanism. This process is reminiscent of the sharpening (narrowing) of spatial receptive fields over the first weeks and months after the onset of experience (DeAngelis et al., 1993b; Tavazoie and Reid, 2000; Kiorpes, 2015, 2016).

Increased intrinsic excitability

As neurons mature, they must regulate their ion channels and synaptic connections in order to bring their spiking response rates into an appropriate physiological range (Turrigiano and Nelson, 2004). At eye opening, neurons *in vivo* exhibit weak spiking activity (Clemens et al., 2012) (this study) and both rats (Kasper et al., 1994) and ferrets (this study) exhibit wide action potentials. Further, as neurons are maturing during this stage just after eye opening, their input resistance also rapidly decreases (Kasper et al., 1994; Desai et al., 2002; Wang et al., 2012), which means the same input current will produce a smaller resulting voltage. Previous studies in rats have shown that layer 4 neurons add synapses during this time (Desai et al., 2002) and that spike threshold decreases (Kasper et al., 1994), presumably to bring the visual response rates up to mature values and to overcome the decreasing input resistance. In other feed-forward systems, the weight of feed-forward connections increases substantially: ~50 fold over the first week of vision at the retinogeniculate synapse (Chen and Regehr, 2000) and 2-4 fold from P4 to P15 in the barrel cortex (Li et al., 2013), presumably to allow mature selectivity and firing rates. Because subthreshold voltage responses increase over the first week of vision and because input resistance is going down, feed-forward synaptic contributions to visual cortex are also likely to be increasing, although we are not aware of direct measurements that would confirm this hypothesis. Increases in sodium channel density at the axon initial segment may underlie the enhancement in the maximum slope of Vm during an action potential (max dV/dt) and decreased threshold observed here (Colbert and Pan, 2002; Kole et al., 2008; Hu et al., 2009; Grubb and Burrone, 2010; Kuba et al., 2010).

While we observed an increase in input-output gain, a reduced spike threshold (*ex vivo*), and evidence of a more excitable membrane (increased maximum dV/dt), we did not observe an

overall increase in spiking in *ex vivo* current-firing rate curves, due to developmental decreases in input resistance. Therefore, it is important to appreciate that the increases in visually-evoked and excitable membrane potential conductances are greater than they initially appear by voltage comparisons across age alone, because they are overcoming a larger passive membrane resistance.

Developmental changes in input-output gain

The spike threshold non-linearity contributes substantially to cortical direction selectivity (Reid et al., 1987; Jagadeesh et al., 1993; Priebe et al., 2004; Priebe and Ferster, 2005). Before these experiments, it was possible to imagine that much of the developmental increase in cortical direction selectivity in ferret might be due not to changes in subthreshold inputs, but rather purely through changes in effective threshold or the voltage-to-firing rate transform (Van Hooser et al., 2014). The experiments here show that increased input-output gain does contribute to the increased firing rates that are observed in experienced animals, but that increased input-output gain did not, by itself, account for the increased direction selectivity index values (see **Figure 7CD**). Instead, changes in the underlying voltage responses were necessary to confer increased direction selectivity.

Possible synaptic bases

It is interesting to consider the possible synaptic bases for the expanded receptive fields we observed here, as we cannot directly examine the physiological properties of the synapses that underlie these receptive fields at this time.

If we consider feed-forward inputs, one could imagine that experience produces new synapses between LGN neurons and cortical neurons, such that newly-connected neurons are providing inputs at the latencies and positions that are newly present in the spatiotemporal receptive fields of mature neurons. Alternatively, maturation of receptive field properties of already-connected LGN neurons or cortical neurons might cause the spatiotemporal receptive field to expand, and confer direction selectivity even without such selectivity in the antecedent inputs. For example, LGN neuron latency drops during the first weeks of visual experience (Tavazoie and Reid, 2000); therefore, it is possible that changes in receptive field properties of already-connected LGN cells that exhibit purely center surround receptive fields could fill out the earlier latency regions of the experienced spatiotemporal receptive fields. Or, perhaps connections from LGN cells with reduced latencies do not form until after the onset of experience. Future experiments could focus on these possibilities.

Although the data here force us to reject the hypothesis that the change in direction selectivity is purely due to postsynaptic changes in excitability, it remains possible that there might be no changes in LGN inputs and that amplified firing from recurrent connections underlie the increases in Vm selectivity (Douglas et al., 1995; Suarez et al., 1995; Christie et al., 2017). Under this view, the enhanced gain in cortical neurons would recurrently drive changes in the synaptic inputs, leading to additional direction selectivity. Further studies will be needed to tease apart the contributions of feed-forward and recurrent connections to direction selectivity.

Materials and Methods

General design: All experimental procedures were approved by the Brandeis University Animal Care and Use Committee and performed in compliance with National Institutes of Health guidelines. In vivo intracellular recordings were carried out in 2 groups of ferrets (*Mustela putorius furo*): "naive" (postnatal day (P) 30-34; n = 10) and "experienced" (P40-60; n = 11).

Sex as a variable: Only female ferrets were used because housing mature male and female ferrets in the same room causes significant hormonal stress for the female animals if they are not allowed to mate.

Surgical preparation: Ferrets were sedated with ketamine (20 mg/kg intramuscular) and given atropine (0.16–0.8 mg/kg intramuscular) and dexamethasone (0.5 mg/kg intramuscular) to reduce bronchial and salivary secretion and to reduce inflammation. Ferrets were next anesthetized with a mixture of isoflurane, oxygen, and nitrous oxide through a mask while a tracheostomy was performed. Ferrets were then ventilated with 1.5–3% isoflurane in a 2:1 mixture of nitrous oxide and oxygen. A cannula was inserted into the intraperitoneal (IP) cavity for delivery of neuromuscular blockers and Ringer's solution (3 ml/kg per hour). The animals were next inserted in a custom stereotaxic frame that did not obstruct vision. All wound margins were infused with bupivacaine. Silicone oil was placed on the eyes to prevent corneal damage. An incision was made on the scalp, a craniotomy performed, and a durotomy performed with a sharp needle (31 gauge). Before recording commenced, ferrets were paralyzed with the neuromuscular blocker gallamine triethiodide (10–30 mg/kg per hour) through the IP cannula to suppress spontaneous eye movements, and the nitrous oxide-oxygen mixture was adjusted to 1:1. The animals' ECG was continuously monitored to ensure adequate anesthesia, and the

percentage of isoflurane was increased if the ECG indicated any distress. Body temperature was maintained at 37°C.

***In vivo* intracellular electrophysiology:** Intracellular recordings were performed using sharp microelectrodes (borosilicate glass, BF100-50-10; Sutter Instruments, CA) with a resistance of 80-120MO when filled with 3M KCl and 5% Neurobiotin at the tip. The electrodes were lowered into the primary visual cortex using a Sutter P-285 micromanipulator. The intracellular potentials were recorded using an AxoClamp 2B amplifier (Molecular Devices, CA) in the bridge mode, and subsequently low-pass filtered at 3 kHz, digitized at 8-11 kHz (micro1401, Cambridge Electronics Design), and stored on a personal computer (PC) hard drive. V1 neurons were recorded between the depths of 230-1100uM, and cells were later classified into simple and complex types based on spike modulation ratio (**Supplementary Figure 2-1**).

Visual stimuli: Visual stimuli were created in MATLAB with the Psychophysics Toolbox (Brainard, 1997; Pelli, 1997; Kleiner et al., 2007) on a Macintosh Pro running OSX and displayed on a Dell monitor 1704FPVt (40 cm viewing distance). Gratings were shown in pseudorandom order at temporal frequencies that varied between 2 – 8 Hz and a spatial frequency of 0.08 cycles per degree, which is in the middle of the maximal response functions for animals in this age range (Li et al., 2006; Popovic et al., 2018). Sparse noise stimuli for reverse correlation analysis were 1-dimensional bar stimuli, rotated so that the bar orientation matched the preferred orientation of each cell (Priebe and Ferster, 2005; Rust et al., 2005). Bar width varied from 1.55-3.1 degrees of visual angle, and bar luminance values were updated each 100ms to be black (10% probability), white (10% probability), or gray (80% probability).

Acute slice electrophysiology: Ferrets (n = 9) were split into naïve (n = 6, age P28-32, 29 cells) and experienced (n = 3, age P41-44, 17 cells) groups. Animals were injected with an intraperitoneal dose of Beuthanasia-D (1 μL/g; 390 mg/mL sodium pentobarbital, 50 mg/mL sodium phenytoin) to induce acute respiratory arrest. Transcardial perfusion was immediately performed using 0.22 M sucrose artificial cerebrospinal fluid (aCSF) that had been chilled to 4° C and aerated in 95% carbon dioxide/5% oxygen gas mixture for 15 minutes. The full composition of the solution used for perfusion and slicing was 220 mM sucrose, 26 mM $NaHCO_3$, 3 mM KCl, 5 mM MgCl, 1.25 mM NaH_2PO_4, 1.0 $CaCl_2$, and 10 mM dextrose. Following decapitation using a small animal guillotine, the brain was extracted, separated into hemispheres and cut again into caudal coronal blocks to excise the occipital lobe before slicing into 330-μm coronal sections on a Leica VT-1000s vibratome at high vibrating frequency in sucrose cutting solution. Sections were retained if fully intact and obtained in the second through the fifth passes in the slicing sequence (i.e. not more than 1650 microns from the extremity of the occipital pole) and most recorded neurons were taken from the second and third slices. Each slice was immediately incubated in aerated standard aCSF (124 mM NaCl, 2.5 mM KCl, 2 mM $MgSO_4$, 1.25 mM $NaHPO_4$, 2 mM $CaCl_2$, 26 mM $NaHCO_3$, 10 mM dextrose, ph 7.4, mOsm 318 ± 2) at 34-35° C for 15-30 minutes and then allowed to recover at room temperature in the same solution for 1 to 1.5 hours. Slices were maintained in an aerated incubation chamber at room temperature until needed for recording when they were transferred to the perfusion chamber and maintained at a temperature of 35° to 37° C during recording.

Current clamp measurements of single neuron intrinsic excitability were obtained in standard ACSF containing 20 μM 6,7-dinitroquinoxaline-2,3-dione (DNQX), either 25 μM of D-2-amino-5-phosphonopentanoate (D-AP-V) or 50 μM of racemic mixture AP-V, and 20 μM of picrotoxin,

synaptic blockers of AMPA, NMDA, and GABA, respectively. A small ad-hoc DC current was injected for all cells to set baseline membrane potential to -60 mV. A series of current pulses were tested over 10 to 15 evenly spaced step sizes between 0 and 400 pA. Single current pulses were 300 too 400 msec in duration over a 1-second acquisition frame with stimulation onset delayed by 50 msec. A 3-second minimum delay was used between all single pulse acquisition frames. The order of current step amplitudes was pseudorandomly interleaved and a minimum of 3 repetitions were acquired for each current level.

Data analysis:

For Vm analysis, spikes were removed from the traces using an 8ms median filter (Ferster and Jagadeesh, 1992). Responses to each stimulus were calculated relative to a baseline that was calculated in the 5 sec preceding each stimulus (or shorter for a few cases where the interstimulus interval was shorter than 5 sec). The baseline was defined as the 20th percentile of the data points in this time interval, to discount any spontaneous activity that was more prevalent especially in the older animals; manual inspection showed that this value was very close to what the experimenter would have selected on a case-by-case basis. For spike analyses, spikes were detected using a manually set threshold on the Vm trace for each recording epoch. For each cell, we examined both the mean response to drifting grating stimulation (F0) as well as the modulation at the stimulus frequency (F1). If a cell's F1 response was greater than the mean response (F0), then the cell was declared to be a "simple" cell. Direction selectivity was examined in recorded cells that exhibited significant variation across all stimuli by an ANOVA test, and tuning curves were fit with a double Gaussian (Mazurek et al., 2014). The direction

selectivity index (DSI) was defined to be (Rp(θ) - Rn(θ))/Rp(θ), where Rp(θ) is the fitted response in the preferred direction (θ) and Rn is the response in the opposite direction 180° + θ.

Reverse correlation with sparse white-noise: Vm traces median-filtered at 8ms to remove spikes as above. For each spatial location, the stimulus trace was cross-correlated (Citron et al., 1981) with the median-filtered Vm trace using the xcorr function in Matlab. Correlation values were plotted as a function of lag time with respect to stimulus onset (time 0). Attempts to sharpen (or whiten) the reverse correlation to remove the blurring from the step-function-like stimuli typically resulted in unstable filters, so only the raw stimulus-voltage correlation waveform is plotted here, as these measurements were always stable.

Subunit analysis: Once the Vm STRFs were computed, pixels clusters representing each ON and OFF subunit were detected through connected component analysis using the *bwconncomp* function in MATLAB. Only the brightest and the darkest 5% of pixels from the STRF images were analyzed using *bwconncomp* for ON and OFF subunits, respectively. To eliminate random pixel clusters spuriously detected by the method, only pixel clusters containing at least 20 pixels were accepted as subunits, and an ellipse was drawn through each accepted pixel cluster to represent a subunit. Next, using the *regionprops* function in MATLAB, the following parameters were extracted for each ellipse: orientation, major axis length, minor axis length, eccentricity and area. Further, using these parameters and the geometric properties of an ellipse, the following parameters were also calculated: spatial extent (the projection of the ellipse on the x or spatial axis), temporal extent (the projection of the ellipse on the y or time axis), maximum latency (the upper bound of the ellipse on the time axis) and minimum latency (the lower bound of the ellipse

on the time axis). Values for each of the above 9 parameters from all ON and OFF subunits from a single cell were averaged to obtain cell-average values.

V-F transform: Vm signals were filtered with a 60Hz Savitzky-Golay filter to remove a small 60Hz component, and spikes were filtered out of Vm by applying an 8ms median filter (Finn et al., 2007) and baseline subtraction as described above. Next, a set of ordered pairs of Vm values and corresponding firing rate values were created by calculating the mean Vm and mean firing rate in non-overlapping 30ms windows that were run across the data (Priebe and Ferster, 2005, 2006). The relationship between these pairs (Vm and firing rate) for each cell was fit by a hyperbolic tangent function: $FR(V) = b * \mathit{rectify}(V-Vth)^{\alpha}$, where α was constrained to be between 1 and 4 and rectify(x) := x, if $x \geq 0$; 0, if $x<0$. Empirical data was plotted against these fits by binning observations into 1 mV bins and computing the mean and standard error of the mean.

Spike kink analysis: Spike "kinks" (a particular definition for spike threshold) were calculated for spikes following the algorithm by Azouz and Gray (1999). In brief, dV/dt was calculated by dividing the difference between successive samples by the time interval between them. The spike kink voltage was defined to be the point at which dV/dt exceeded 0.033 of the maximum value.

Table 1. Key Resources Table

Reagent type	Designation	Source or reference	Identifiers	Additional information
Software	Matlab	The MathWorks, Natick, MA	RRID: SCR_001622	

Software	GitHub	GitHub	RRID: SCR_002630	
Software	Psychophysics Toolbox	Psychtoolbox.org	RRID: SCR_002881	
Software	Spike2	Cambridge Electronic Design		
Hardware and software	Spyder Express 3	Datacolor		
Microscope				
Animals	Ferrets	Marshall Bio-resources	“Conventional” colony	
Lab equipment	Electrode Puller	Sutter Instrument Company	P-97 with box filament	
Lab equipment	Micromanipulator	Sutter Instrument Company	MP-285	
Lab equipment	Microelectrode amplifier	Axon Instruments (now Molecular Devices)	AxoClamp-2B	
Lab equipment	Multifunction data acquisition system	Cambridge Electronic Design	Micro1401	

Figures and legends

Figure 1

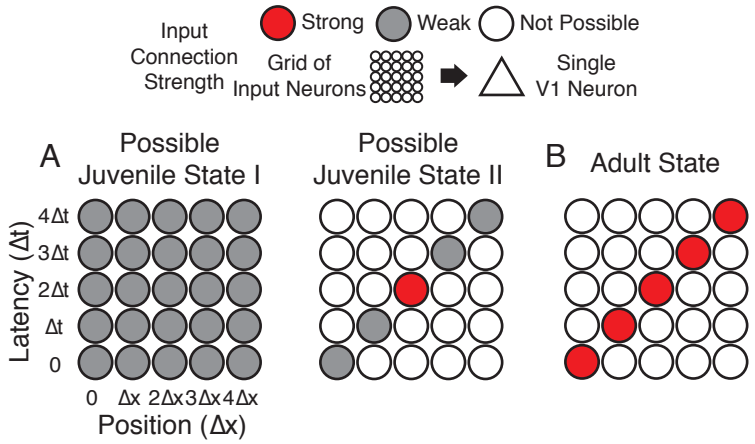

Figure 1. Hypotheses of initial naïve states. A) In Possible Juvenile State I, receptive fields might be initially broad and weak in space and time and later sharpened to exhibit a slant. In this state, the lack of direction selectivity comes from the symmetry in the broad initial receptive field. In Possible Juvenile State II, there is a compact initial input that is constrained to grow only at certain positions and latencies. In this state, the lack of direction selectivity comes from the symmetry of compact strong input, and the weak inputs do not contribute at the naïve stage. **B)** Experienced state, with a characteristic directional slant in space time, indicating that the cell would respond to a leftward moving stimulus at an appropriate velocity.

Figure 2

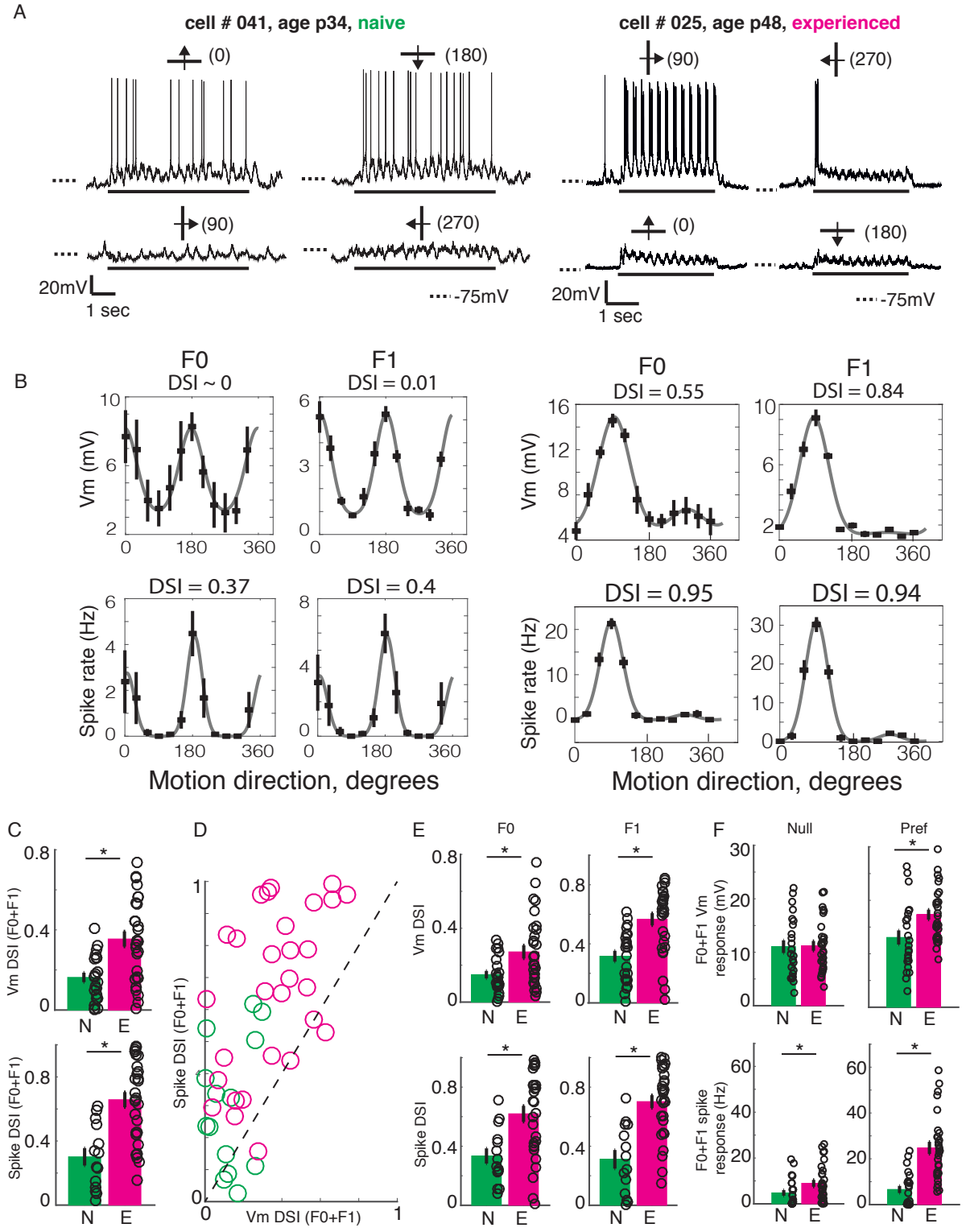
A
cell # 041, age p34, naive
cell # 025, age p48, experienced
(0)
(180)
(90)
(270)
20mV
1 sec
-75mV
B
F0
F1
DSI ~ 0
DSI = 0.01
DSI = 0.55
DSI = 0.84
DSI = 0.37
DSI = 0.4
DSI = 0.95
DSI = 0.94
Vm (mV)
Spike rate (Hz)
Motion direction, degrees
C
D
E
F
Null
Pref
Vm DSI (F0+F1)
Spike DSI (F0+F1)
Vm DSI
Spike DSI
F0+F1 Vm response (mV)
F0+F1 spike response (Hz)
N
E

Figure 2. Developmental increase in direction selectivity of membrane potential (Vm) and spiking responses in V1 cells. A) Vm responses of a simple cell from a visually naïve and an experienced ferret each. For each cell, single-trial responses to presentation of sinusoidal gratings moving in both directions orthogonal to the preferred orientation (top) and the non-preferred orientation (bottom) are shown. The stimulus orientations and motion directions are indicated above each trace with a solid bar and arrow, respectively, and the angles representing the specific directions of motion are given in parentheses. Solid bar below each trace indicates the duration of the stimulus display and dotted lines indicate the Vm level of -75 mV. For both cells, the gratings drifted at a temporal frequency of 4 Hz and the Vm oscillated at the same frequency with a strong response to each grating cycle. **B)** Direction tuning curves of the cells in **A**, plotted separately for Vm (top) and spiking (bottom) responses, and for the F0 or DC (left) and the F1 or fundamental (right) components of the responses. Direction selectivity index (DSI) value calculated from each tuning curve is given above each curve. Both F0 and F1 DSI values are higher in the cell from the experienced animal. **C)** Mean total Vm and spike DSI values, calculated from F0+F1 responses, compared between naïve (N, green) and experienced (E, magenta) animal groups. **D)** Vm and spike total DSI (F0+F1) values for each cell plotted against each other. Dashed line denotes the line of unity. **E)** Same as **C**, but the DSI values are calculated separately for the F0 and the F1 components of response. **F)** Mean total (F0+F1) Vm and spiking responses to the null and preferred direction of motion compared between naïve and experienced groups. For all panels: error bars denote SEM; circles denote values for individual cells; asterisks denote significant differences at $p < 0.05$ level, Wilcoxon rank sum test.

Supplementary Figure 2-1

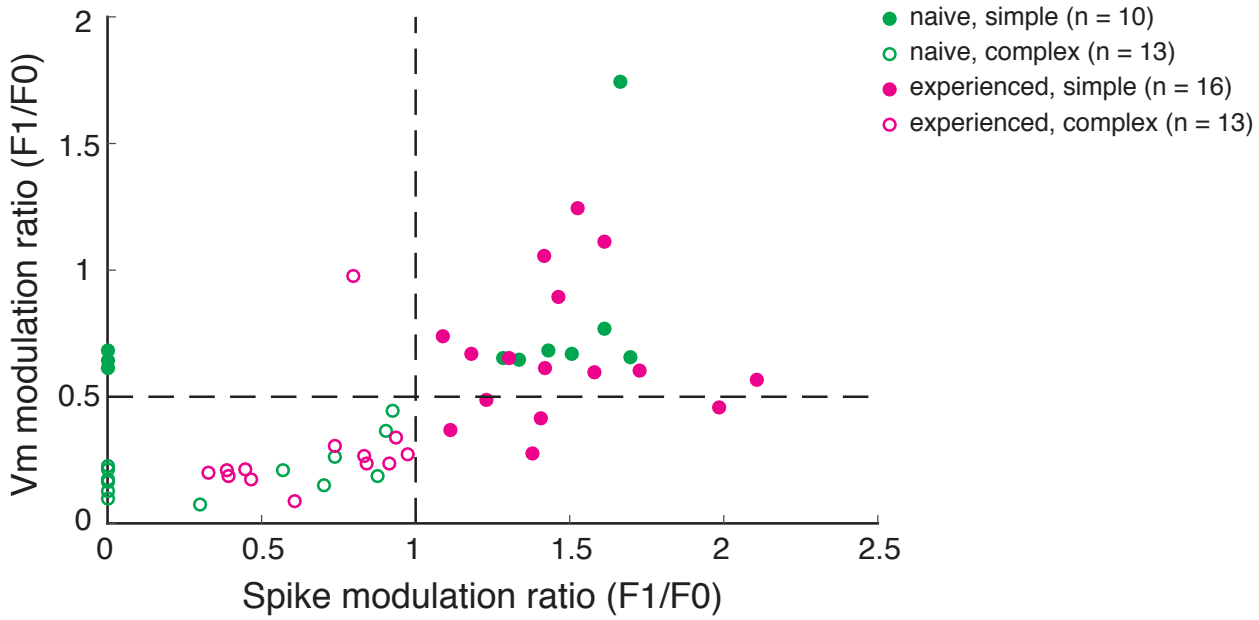

Supplementary Figure 2-1. Scatterplot of spike and Vm modulation ratios (F1/F0) for all cells recorded. Cells with spike modulation ratio > 1 from this figure were classified as simple cells. In the naïve group, many neurons did not fire sufficient spikes to calculate a spike modulation ratio. Those neurons were plotted in this figure with a spole modulation ratio set to 0. Out of those neurons, those with Vm modulation ratio > 0.5 were classified as simple cells.

Figure 3

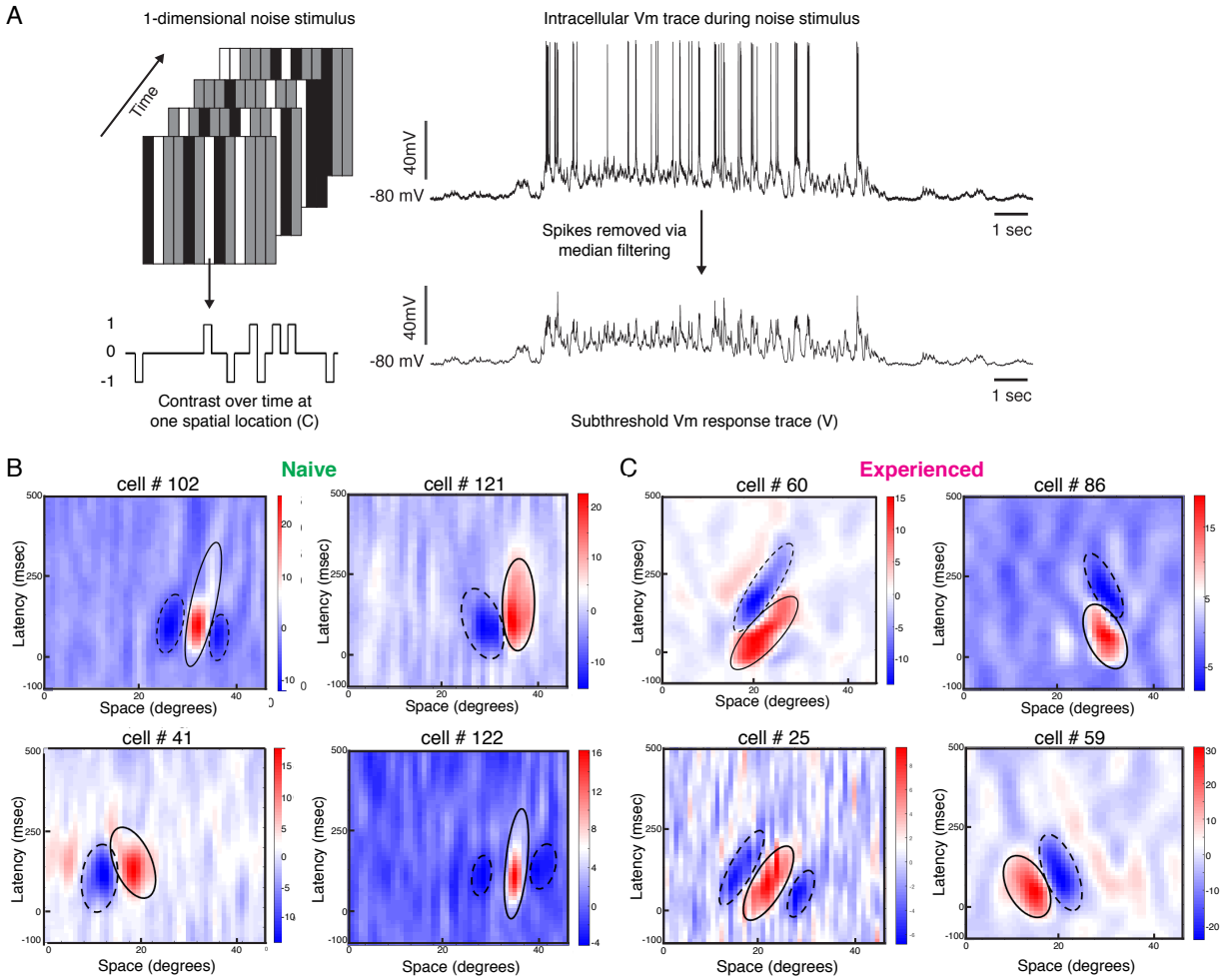

Figure 3. Developmental reorganization of linear spatiotemporal receptive fields in visual cortical simple cells. A) Schematic of sparse noise stimulus, rotated to match each cell's preferred orientation. Spikes were removed and the membrane potential was correlated with the stimulus at each position. **B)** Vm spatiotemporal receptive fields of 4 simple cells each from naïve animals. X-axis represents spatial location, y-axis represents latency from onset of visual stimuli, and the cross-correlation coefficient between the stimulus contrast and Vm values are represented by the color. Black lines outline the ellipses fitted to the ON (continuous) and OFF (dashed) subunits. Raw correlations are shown, which are blurred by the time step of the stimulus (100ms), so some ellipses overlap zero. **C)** Same, for 4 cells from experienced animals. Receptive fields in experienced animals appeared more elongated in space time, and more slanted, consistent with the increased direction selectivity that was observed.

Figure 4

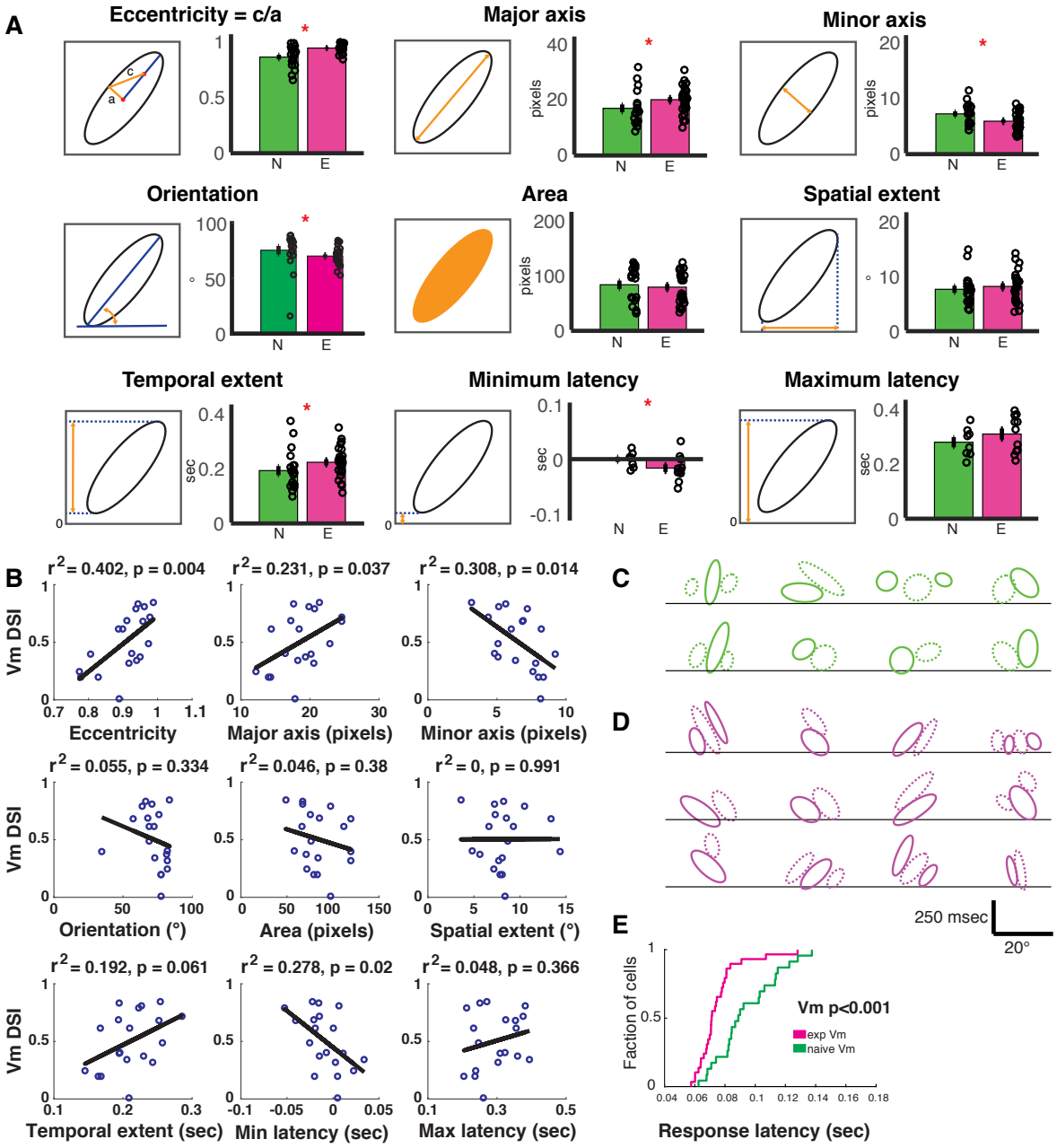

Figure 4. Spatiotemporal receptive fields become more extended, slanted in space-time with short-term visual experience. A) Quantification of the 9 parameters defining the characteristics of the spatiotemporal receptive field subunits. In each panel, the parameter being quantified is described by a schematic on the left, and on the right is a bar plot showing the mean ± SEM of the parameter values in the naïve (N, green, 19 subunits from 8 cells) and experienced (E, purple, 26 subunits from 12 cells) animals. Black circles denote individual subunit values. Red stars denote statistical significance at $p < 0.05$ level via WRS test. **B)** Relationship between cell-average spatiotemporal receptive field structure parameters and Vm DSI for all simple cells. The R^2 and p values for each linear correlation are shown above each plot. Raw correlations were

used in the calculations, which are blurred by the time step of the stimulus (100ms), so some ellipses begin earlier than 0. **C)** All subunits (ON=solid, OFF=dashed) for naïve cells. Lines are at 0 time lag. Scale bar shows 250 msec by 20° of visual angle. Note that correlations are raw, so they are blurred 100ms by the stimulus timesteps (some subunits begin before time 0). **D)** Same, for experienced cells. Note the earlier onset responses and the greater slants. **E)** Cumulative histogram of response latencies of naïve and experienced simple cells to grating stimuli. Latency is defined as the first time when the voltage signal reaches 6 standard deviations.

Figure 5

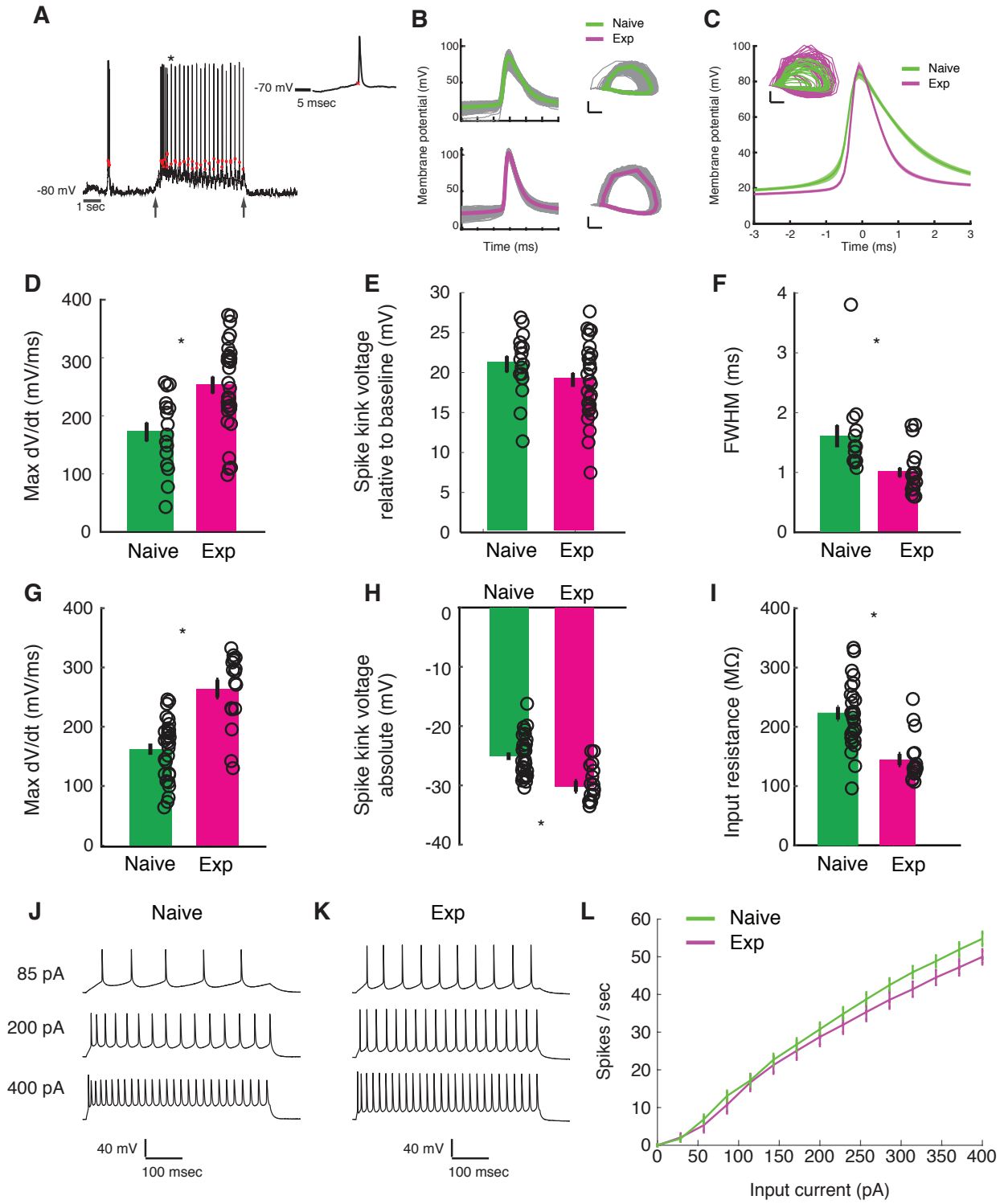
A
-70 mV
5 msec
-80 mV
1 sec
B
Naive
Exp
Membrane potential (mV)
Time (ms)
C
Naive
Exp
Membrane potential (mV)
Time (ms)
D
Max dV/dt (mV/ms)
Naive
Exp
E
Spike kink voltage relative to baseline (mV)
Naive
Exp
F
FWHM (ms)
Naive
Exp
G
Max dV/dt (mV/ms)
Naive
Exp
H
Naive
Exp
Spike kink voltage absolute (mV)
I
Input resistance (MΩ)
Naive
Exp
J
Naive
85 pA
200 pA
400 pA
40 mV
100 msec
K
Exp
40 mV
100 msec
L
Naive
Exp
Spikes / sec
Input current (pA)

Figure 5. Developmental enhancement of excitability in cortical cells. A) Detection of spike kink voltage from single action potentials *in vivo* (Azouz and Gray, 1999). **B)** Action potentials and spike phase diagram from an example naïve (top) and experienced cell (bottom). Individual spike traces shown in gray. In spike phase diagram, membrane potential is on the horizontal axis (scale bar is 20mV) and dV/dt is on the vertical axis (scale bar is 100 mV/msec). **C)** Average and standard error of the mean of voltage waveforms for naïve (N=14) and experienced (N=29) cells, showing much wider action potentials in naïve animals. Shaded area is standard error of the mean across cells. Inset: phase diagram of mean spike waveforms; membrane potential is on the horizontal axis (scale bar is 20mV) and dV/dt is on the vertical axis (scale bar is 100 mV/msec). **D)** Maximum dV/dt for naïve and experienced cells *in vivo* (WRS test, P<2.0e-04); **E)** spike kink voltages *in vivo* (WRS test, P=0.2); **F)** action potential full width at half height (WRS test, P<4.3e-04) *in vivo*. **G)** Maximum dV/dt for synaptically-isolated cells in brain slices for naïve and experienced animals. *Ex vivo* measurements showed similar maximum dV/dt values as *in vivo* measurements (N=29 naïve, N=17 experienced, WRS, P<2.4e-05), showing similar values as *in vivo* measurements. **H)** Spike kink voltage exhibited a significant decrease when measured in isolated cells from visually experienced animals (WRS P<1.6e-04). **I)** Spike kink reductions and increased maximum dV/dt co-occurred with developmentally-typical decreases in membrane resistance (WRS, P<1.2e-04), suggesting that experienced cells would take longer to charge from rest even though they spike at lower voltages. Example firing rate vs. current curves for a cell from a naïve (**J**) animal and an experienced (**K**) animal are shown, and average firing rate vs. current curves are shown (**L**). The increased excitability with age and the decreased input resistance produced firing rate vs. current relationships that were not different between the 2 cases: (Kruskal-Wallis test of slopes: P<0.068). For all panels, P-values as listed are before Bonferroni correction; significant * indicates significant difference after Bonferroni correction (which did not change results for these tests).

Figure 6

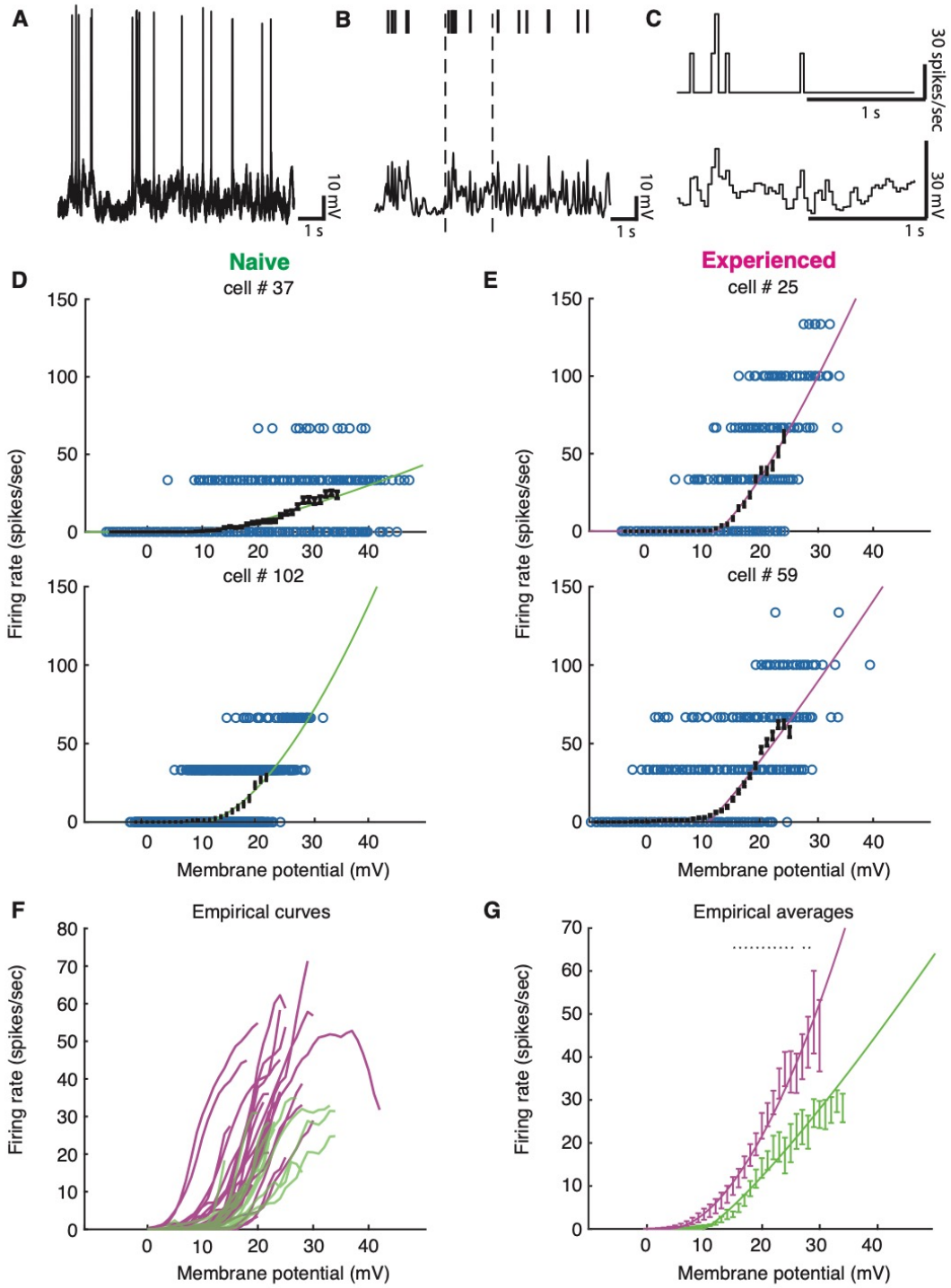

Figure 6. Developmental enhancement of input-output gain. A) To calculate the voltage-to-firing rate transform, we **B)** extracted spike times and used median filtering to remove spike waveforms from the membrane potential, and **C)** averaged firing rate and spike-filtered membrane potential into 30 msec bins (Priebe et al., 2004; Priebe and Ferster, 2005, 2006). **D)**

Membrane potential and firing rate observations from 2 cells from naïve and **E)** 2 cells from experienced animals. Empirical means and standard error of the mean in sliding 1mV windows (black) and a power law fit (Priebe et al., 2004) (naïve are green, experienced are magenta) are shown for each cell. Empirical means are calculated up until first bin that does not contain 15 Vm, firing rate ordered pairs. **F)** Empirical mean voltage-to-firing rate relationships for all cells (N=16 naïve, N=29 experienced). **G)** Mean and standard error of the mean empirical voltage-to-firing rate transforms for naïve and experienced animals, averaging over cells; * indicates locations where a t-test shows a p-value of less than 0.05. Voltage values that had data for at least 2 cells are shown. Experienced voltage-to-firing rate transforms exhibited increased firing rates at a given voltage over a large membrane voltage range. Solid lines are power law fits, weighed by number of data points at each voltage.

Supplementary Figure 6-1

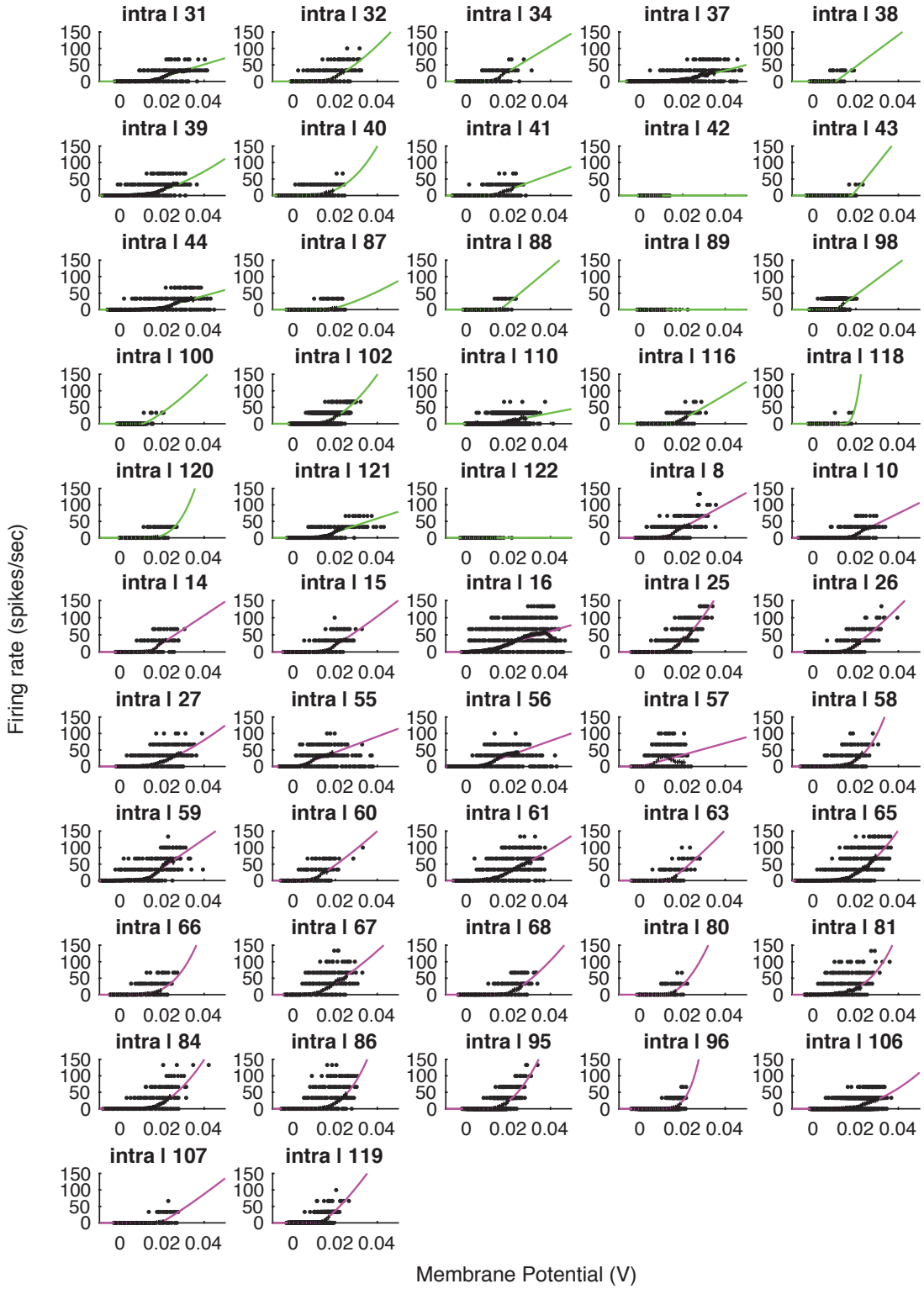

Supplementary Figure 6-1. Voltage-to-firing rate transforms for all cells in the study. This figure includes all cells, including cells that exhibited no 1mV bin with at least 15 spikes (inclusion criteria for the group analysis).

Figure 7

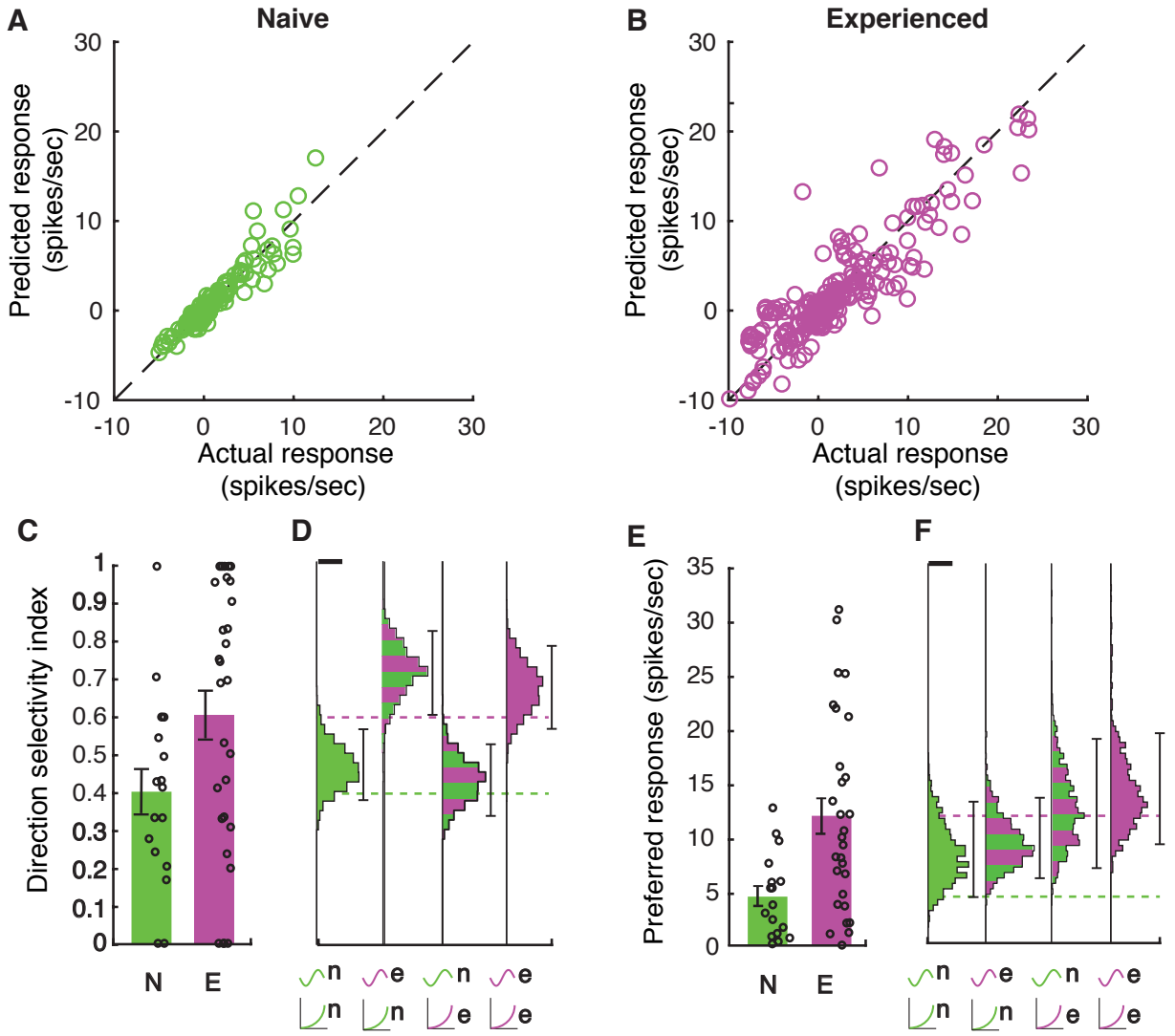

Figure 7. Increases in membrane potential selectivity and input-output gain are both required for mature direction selectivity and firing rates. A) Actual mean spiking response rates for each stimulus plotted against the mean spiking response that is obtained by applying the voltage-to-firing rate transform to each stimulus's membrane potential record for all naïve cells (N=16), showing that the phenomenological model captures the voltage-to-membrane transfer well. **B)** Same, for experienced cells (N=29). Model captures the actual spiking responses well. **C)** Actual direction index values derived from the mean responses (F0) of naïve and experienced cells. **D)** Simulations of what we would expect if naïve or experienced waveforms were paired with naïve or experienced voltage-to-firing rate transforms. Plots show vertical histograms (with 5-95 percentile error bars) of mean direction selectivity index values for 10000 simulations of 20 cells for several cases: 1) randomly selected naïve voltage waveforms applied to randomly selected naïve voltage-to-firing rate transforms; 2) randomly selected experienced voltage waveforms applied to randomly selected naïve voltage-to-firing rate transforms; 3) randomly

selected naïve voltage waveforms applied to randomly selected experienced voltage-to-firing rate transforms, and 4) randomly selected experienced voltage waveforms applied to randomly selected experienced voltage-to-firing rate transforms. Scale bar on top of histogram shows 100 simulations. Axis labels identify the model by the waveforms used (top symbol) and voltage-to-firing rate transform used (bottom symbol). Actual data values are shown as dashed lines. To achieve increases in direction selectivity, it was only necessary for the model to adopt the voltage response waveforms of the experienced animals: the increased gain of the experienced animals was not necessary. **E+F)** Same as **C,D**, but response to preferred direction is shown. Scale bar shows 50 simulations. To achieve increases in firing rates observed in experienced animals, experienced voltage-to-firing rate transforms were necessary. In **D**,**F**, models can be compared to whether they match the individual cell data by seeing if the individual cell data mean across cells falls within the 5-95%-tile range (the distribution of means is sampled empirically through simulation). Overall, to achieve both increases in direction selectivity and firing rate that are observed *in vivo*, changes in voltage responses and voltage-to-firing rate transform were necessary.

References

Azouz R, Gray CM (1999) Cellular mechanisms contributing to response variability of cortical neurons. J Neurosci 19:2209-2223.

Brainard DH (1997) The Psychophysics Toolbox. *Spatial Vision* 10:433-436.

Brown MC, Jansen JKS, Van Essen D (1976) Polyneuronal innervation of skeletal muscle in new-born rats and its elimination during maturation. J Physiology 261:387-422.

Cang J, Niell CM, Liu X, Pfeiffenberger C, Feldheim DA, Stryker MP (2008) Selective disruption of one Cartesian axis of cortical maps and receptive fields by deficiency in ephrin-As and structured activity. Neuron 57:511-523.

Carandini M, Ferster D (2000) Membrane potential and firing rate in cat primary visual cortex. J Neurosci 20:470-484.

Changeux JP, Danchin A (1976) Selective stabilization of developing synapses as a mechanisms for the specification of neuronal networks. Nature 264:705-712.

Chapman B, Stryker MP (1993) Development of orientation selectivity in ferret visual cortex and effects of deprivation. J Neurosci 13:5251-5262.

Chen C, Regehr WG (2000) Developmental remodeling of the retinogeniculate synapse. Neuron 28:955-966.

Christie IK, Miller P, Van Hooser SD (2017) Cortical amplification models of the experience-dependent development of selective columns and response sparsification. J Neurophysiol:jn 00177 02017.

Citron MC, Kroeker JP, McCann GD (1981) Nonlinear interactions in ganglion cell receptive fields. J Neurophysiol 46:1161-1176.

Clemens JM, Ritter NJ, Roy A, Miller JM, Van Hooser SD (2012) The laminar development of direction selectivity in ferret visual cortex. J Neurosci 32:18177-18185.

Colbert CM, Pan E (2002) Ion channel properties underlying axonal action potential initiation in pyramidal neurons. Nat Neurosci 5:533-538.

Crair MC, Gillespie DC, Stryker MP (1998) The role of visual experience in the development of columns in cat visual cortex. Science 279:566-570.

DeAngelis GC, Ohzawa I, Freeman RD (1993a) Spatiotemporal organization of simple-cell receptive fields in the cat's striate cortex. II. Linearity of temporal and spatial summation. J Neurophysiol 69:1118-1135.

DeAngelis GC, Ohzawa I, Freeman RD (1993b) Spatiotemporal organization of simple-cell receptive fields in the cat's striate cortex. I. General characteristics and postnatal development. J Neurophysiol 69:1091-1117.

Desai NS, Cudmore RH, Nelson SB, Turrigiano GG (2002) Critical periods for experience-dependent synaptic scaling in visual cortex. Nat Neurosci 5:783-789.

Douglas RJ, Koch C, Mahowald M, Martin KA, Suarez HH (1995) Recurrent excitation in neocortical circuits. Science 269:981-985.

Durack JC, Katz LC (1996) Development of horizontal projections in layer 2/3 of ferret visual cortex. Cereb Cortex 6:178-183.

Erisir A, Harris JL (2003) Decline of the critical period of visual plasticity is concurrent with the reduction of NR2B subunit of the synaptic NMDA receptor in layer 4. J Neurosci 23:5208-5218.

Ferster D, Jagadeesh B (1992) EPSP-IPSP interactions in cat visual cortex studied with in vivo whole-cell patch recording. J Neurosci 12:1262-1274.

Finn IM, Priebe NJ, Ferster D (2007) The emergence of contrast-invariant orientation tuning in simple cells of cat visual cortex. Neuron 54:137-152.
Grubb MS, Burrone J (2010) Activity-dependent relocation of the axon initial segment fine-tunes neuronal excitability. Nature 465:1070-1074.
Gu Y, Cang J (2016) Binocular matching of thalamocortical and intracortical circuits in the mouse visual cortex. eLife 5.
Hatta S, Kumagami T, Qian J, Thornton M, Smith EL, 3rd, Chino YM (1998) Nasotemporal directional bias of V1 neurons in young infant monkeys. Invest Ophthalmol Vis Sci 39:2259-2267.
Hu W, Tian C, Li T, Yang M, Hou H, Shu Y (2009) Distinct contributions of Na(v)1.6 and Na(v)1.2 in action potential initiation and backpropagation. Nat Neurosci 12:996-1002.
Huttenlocher PR (1979) Synaptic density in human frontal cortex - developmental changes and effects of aging. Brain Res 163:195-205.
Huttenlocher PR (1990) Morphometric study of human cerebral cortex development. Neuropsychologia 28:517-527.
Jagadeesh B, Wheat HS, Ferster D (1993) Linearity of summation of synaptic potentials underlying direction selectivity in simple cells of the cat visual cortex. Science 262:1901-1904.
Kasper EM, Larkman AU, Lübke J, Blakemore C (1994) Pyramidal neurons in layer 5 of the rat visual cortex. II. Development of electrophysiological properties. J1 Comp1 Neurol 339:475-494.
Katz LC, Shatz CJ (1996) Synaptic activity and the construction of cortical circuits. Science 274:1133-1138.
Kiorpes L (2015) Visual development in primates: Neural mechanisms and critical periods. Dev Neurobiol 75:1080-1090.
Kiorpes L (2016) The Puzzle of Visual Development: Behavior and Neural Limits. J Neurosci 36:11384-11393.
Kleiner M, Brainard D, Pelli D (2007) "What's new in Psychtoolbox-3?". Perception 36:ECVP Abstract Supplement.
Kole MH, Ilschner SU, Kampa BM, Williams SR, Ruben PC, Stuart GJ (2008) Action potential generation requires a high sodium channel density in the axon initial segment. Nat Neurosci 11:178-186.
Kuba H, Oichi Y, Ohmori H (2010) Presynaptic activity regulates Na(+) channel distribution at the axon initial segment. Nature 465:1075-1078.
Leong JC, Esch JJ, Poole B, Ganguli S, Clandinin TR (2016) Direction Selectivity in Drosophila Emerges from Preferred-Direction Enhancement and Null-Direction Suppression. J Neurosci 36:8078-8092.
Li H, Fertuzinhos S, Mohns E, Hnasko TS, Verhage M, Edwards R, Sestan N, Crair MC (2013) Laminar and columnar development of barrel cortex relies on thalamocortical neurotransmission. Neuron 79:970-986.
Li Y, Fitzpatrick D, White LE (2006) The development of direction selectivity in ferret visual cortex requires early visual experience. Nat Neurosci 9:676-681.
Li Y, Van Hooser SD, Mazurek M, White LE, Fitzpatrick D (2008) Experience with moving visual stimuli drives the early development of cortical direction selectivity. Nature 456:952-956.
Livingstone MS (1998) Mechanisms of direction selectivity in macaque V1. Neuron 20:509-526.

Mazurek M, Kager M, Van Hooser SD (2014) Robust quantification of orientation selectivity and direction selectivity. Front Neural Circuits 8:92.
McLean J, Raab S, Palmer LA (1994) Contribution of linear mechanisms to the specification of local motion by simple cells in areas 17 and 18 of the cat. Visual Neurosci 11:271-294.
Mechler F, Ringach DL (2002) On the classification of simple and complex cells. Vision Res 42:1017-1033.
Meliza CD, Dan Y (2006) Receptive-field modification in rat visual cortex induced by paired visual stimulation and single-cell spiking. Neuron 49:183-189.
Miller KD, Keller JB, Stryker MP (1989) Ocular dominance column development: Analysis and simulation. Science 245:605-615.
Pelli DG (1997) The VideoToolbox software for visual psychophysics: Transforming numbers into movies. *Spatial Vision* 10:437-442.
Petanjek Z, Judas M, Simic G, Rasin MR, Uylings HB, Rakic P, Kostovic I (2011) Extraordinary neoteny of synaptic spines in the human prefrontal cortex. Proc Natl Acad Sci U S A 108:13281-13286.
Popovic M, Stacy AK, Kang M, Nanu R, Oettgen CE, Wise DL, Fiser J, Van Hooser SD (2018) Development of Cross-Orientation Suppression and Size Tuning and the Role of Experience. J Neurosci 38:2656-2670.
Press WH, Flannery BP, Teukolsky SA, Vetterling WT (1993) Numerical recipes in C. Cambridge: Cambridge University Press.
Priebe NJ, Ferster D (2005) Direction selectivity of excitation and inhibition in simple cells of the cat primary visual cortex. Neuron 45:133-145.
Priebe NJ, Ferster D (2006) Mechanisms underlying cross-orientation suppression in cat visual cortex. Nat Neurosci 9:552-561.
Priebe NJ, Mechler F, Carandini M, Ferster D (2004) The contribution of spike threshold to the dichotomy of cortical simple and complex cells. Nat Neurosci 7:1113-1122.
Purves D, Lichtman JW (1980) Elimination of synapses in the developing nervous system. Science 210:153-157.
Reichardt W (1987) Evaluation of optical motion information by movement detectors. J Comp Physiol A 161:533-547.
Reichardt W, Poggio T (1976) Visual control of orientation behaviour in the fly. Quart Rev Biophys 9:311-375.
Reid RC, Soodak RE, Shapley RM (1987) Linear mechanisms of directional selectivity in simple cells of cat striate cortex. Proc Natl Acad Sci U S A 84:8740-8744.
Reid RC, Soodak RE, Shapley RM (1991) Directional selectivity and spatiotemporal structure of receptive fields of simple cells in cat striate cortex. J Neurophysiol 66:505-529.
Reid RC, Victor JD, Shapley RM (1997) The use of m-sequences in the analysis of visual neurons: linear receptive field properties. Vis Neurosci 14:1015-1027.
Ringach DL, Sapiro G, Shapley R (1997) A subspace reverse-correlation technique for the study of visual neurons. Vision Res 37:2455-2464.
Ritter NJ, Anderson NM, Van Hooser SD (2017) Visual Stimulus Speed Does Not Influence the Rapid Emergence of Direction Selectivity in Ferret Visual Cortex. J Neurosci 37:1557-1567.
Rochefort NL, Narushima M, Grienberger C, Marandi N, Hill DN, Konnerth A (2011) Development of direction selectivity in mouse cortical neurons. Neuron 71:425-432.

Rust NC, Schwartz O, Movshon JA, Simoncelli EP (2005) Spatiotemporal elements of macaque v1 receptive fields. Neuron 46:945-956.
Ruthazer ES, Stryker MP (1996) The role of activity in the development of long-range horizontal connections in area 17 of the ferret. J Neurosci 16:7253-7269.
Smith GB, Hein B, Whitney DE, Fitzpatrick D, Kaschube M (2018) Distributed network interactions and their emergence in developing neocortex. Nat Neurosci 21:1600-1608.
Smith GB, Sederberg A, Elyada YM, Van Hooser SD, Kaschube M, Fitzpatrick D (2015) The development of cortical circuits for motion discrimination. Nat Neurosci 18:252-261.
Suarez H, Koch C, Douglas R (1995) Modeling direction selectivity of simple cells in striate visual cortex within the framework of the canonical microcircuit. J Neurosci 15:6700-6719.
Tavazoie SF, Reid RC (2000) Diverse receptive fields in the lateral geniculate nucleus during thalamocortical development. Nat Neurosci 3:608-616.
Turrigiano GG, Nelson SB (2004) Homeostatic plasticity in the developing nervous system. Nat Rev Neurosci 5:97-107.
Van Hooser SD, Escobar GM, Maffei A, Miller P (2014) Emerging feed-forward inhibition allows the robust formation of direction selectivity in the developing ferret visual cortex. J Neurophysiol 111:2355-2373.
Van Hooser SD, Li Y, Christensson M, Smith GB, White LE, Fitzpatrick D (2012) Initial neighborhood biases and the quality of motion stimulation jointly influence the rapid emergence of direction preference in visual cortex. J Neurosci 32:7258-7266.
van Kleef JP, Stange G, Ibbotson MR (2010) Applicability of white-noise techniques to analyzing motion responses. J Neurophysiol 103:2642-2651.
Wang BS, Sarnaik R, Cang J (2010) Critical period plasticity matches binocular orientation preference in the visual cortex. Neuron 65:246-256.
Wang L, Fontanini A, Maffei A (2012) Experience-dependent switch in sign and mechanisms for plasticity in layer 4 of primary visual cortex. J Neurosci 32:10562-10573.
White LE, Fitzpatrick D (2007) Vision and cortical map development. Neuron 56:327-338.
White LE, Coppola DM, Fitzpatrick D (2001) The contribution of sensory experience to the maturation of orientation selectivity in ferret visual cortex. Nature 411:1049-1052.
Whitney D, Chang JT, Fitzpatrick D (2019) Experience-dependent reorganization drives development of a binocularly unified cortical representation of orientation. bioRxiv:761395.